Processing and Application of Ceramics 16 [1] (2022) 48–54
https://doi.org/10.2298/PAC2201048Y

Influence of V_2O_5 and B_2O_3 addition on the sintering behaviour and physical properties of ZnO ceramics

Berat Yüksel Price[1,*], Gökhan Hardal[2], Barış Kınacı[3,4]

[1]*Department of Metallurgical and Materials Engineering, Engineering Faculty, Istanbul University-Cerrahpaşa, 34320, Istanbul, Turkey*
[2]*Technology Transfer Centre (TTC), Istanbul University, Istanbul, Turkey*
[3]*Department of Physics, Faculty of Science, Istanbul University, 34134, Istanbul, Turkey*
[4]*Photonics Research Center, Gazi University, 06500, Ankara, Turkey*

Received 5 July 2021; Received in revised form 3 December 2021; Accepted 7 February 2022

Abstract

The effect of V_2O_5 and B_2O_3 additions on sintering behaviour and physical properties of ZnO ceramics was investigated. XRD studies revealed ZnO as main phase with a hexagonal wurtzite-type structure. The V_2O_5 addition is the reason for an increase in grain size and some grains of oblong shape morphology in the ZnO ceramics. The dual addition of V_2O_5-B_2O_3 improved the liquid-assisted sintering of ZnO ceramics and resulted in further increase in grain size with more uniform grain growth. The reduction of sintering temperature to 900 °C for ZnO ceramics was observed with the dual addition of V_2O_5 and B_2O_3. The room temperature PL spectra of the Z (ZnO), ZV (ZnO with 0.5 mol% V_2O_5) and ZVB (ZnO with 0.5 mol% V_2O_5 and 0.5 mol% B_2O_3) ceramics revealed broad visible emission band because of impurities and defects in ZnO ceramics caused by oxygen vacancies due to vanadium and boron additions, as well as zinc interstitials. This emission band between 450–750 nm includes the entire visible region from blue to red.

Keywords: *boron oxide, ceramics, sintering, vanadium pentoxide, zinc oxide*

I. Introduction

Zinc oxide is a unique material for UV emitter devices [1], gas sensors [2], solar cells [3], piezoelectric transducers [4] and varistors [5] owing to its remarkable optical and electrical properties. Zinc oxide with some metal oxides addition such as Bi_2O_3, MnO_2, V_2O_5 and Co_3O_4 shows nonlinear current-voltage (*I-V*) characteristics which is ideally suited for varistor applications. Among numerous varistor systems, ZnO-V_2O_5 ceramic system can be fabricated at a relatively low sintering temperature of about 900 °C. This is very essential advantage for the applications in multilayer components. ZnO ceramics with V_2O_5 can be sintered with a silver electrode (with melting point 961 °C) without a need to use the expensive metals and they can reach the same density at a lower temperature compared to Bi_2O_3-doped ZnO materials [5–11].

Zinc oxide-based materials are also a potential material for the optoelectronic devices [12,13]. The visible emission of ZnO thin films is associated with different intrinsic defects [14]. It was also reported that ZnO-V_2O_5 composites showed excellent optical properties [15]. According to the results of another report, the photocatalytic efficiency under visible light irradiation can be improved by the V_2O_5 addition into ZnO [16].

Furthermore, n-type semi-conductivity of ZnO ceramics is based on trivalent dopant, such as B, Al, In and Ga. Owing to the exceptional combination of physical properties, ZnO is a good candidate for various industrial applications [17]. In our previous work, we reported that the addition of small amount of B_2O_3 up to 1 mol% to ZnO as sintering aid was beneficial for lowering the sintering temperature and developing of grain growth [18]. This effect is also important as the electrical properties can also be altered by the microstructural improvement of ZnO ceramics during sintering. In this study, we report on the effect of V_2O_5 and B_2O_3 dual addition on the sintering behaviour and physical properties

* Corresponding author: tel: +90 2124737070 / 17647,
e-mail: *berat@iuc.edu.tr*

of ZnO ceramics produced by the conventional ceramic processing.

II. Experimental procedure

ZnO (≥99% purity, Merck), V_2O_5 (98.5% purity, BDH) and H_3BO_3 (≥99.5% purity, Merck) powders were used as precursors. Three compositions, ZnO (Z), ZnO with 0.5 mol% V_2O_5 (ZV) and ZnO with 0.5 mol% V_2O_5 and 0.5 mol% B_2O_3 (ZVB), were fabricated by the traditional ceramic processing technique using following steps as mixing, drying, pressing and sintering. The Z and ZV precursor powders were prepared only by ball milling in a nylon jar, whereas for the ZVB sample 1 mol% H_3BO_3 (corresponding to 0.5 mol% B_2O_3) was dissolved in distilled water by continuous stirring and then mixed and milled with 99.5 mol% ZnO + 0.5 mol% V_2O_5 powders. The mixtures were ball milled for 6 h at a rotation speed of 125 rpm using zirconium balls and high purity water. The mixtures were dried at 110 °C in a drying oven and then sifted through a 0.5 mm sieve. The powders were pressed at 100 MPa to prepare samples as discs of 22 mm diameter and 3–4 mm thickness. The samples were sintered in air at 900 °C for 1 h using 6 °C/min heating rate and then cooled spontaneously in furnace for about 8 h [5,7].

Bulk density measurements of the sintered samples were performed with the Archimedes principle method. Phase composition in the samples after sintering was determined by X-ray diffraction analysis (XRD-Rigaku D/Max-2200/PC) using CuKα, scanning angle 2θ from 20° to 80°. The lattice parameters (a and c) of the sintered samples for ZnO phase (hexagonal wurtzite structure) were calculated using the following equation:

$$\sin^2\theta = \frac{\lambda^2}{4}\left[\frac{4}{3}\frac{h^2+k^2+hk}{a^2} + \frac{l^2}{c^2}\right] \quad (1)$$

Fourier transform infra-red spectra (FTIR) of the samples were determined using a Bruker Vertex 80 IR spectrometer in the range of 1500–500 cm^{-1}. The microstructure of the samples on the fractured surfaces was investigated by a scanning electron microscope (SEM, JEOL-JSM 5600). Photoluminescence spectroscopy (PL) measurements of the samples were investigated using the Jobin Yvon Fluorolog-550 PL system with a 50 mW HeCd laser (λ = 325 nm) as excitation light source at room temperature.

III. Results and discussion

XRD patterns of the ZnO (Z), ZnO with 0.5 mol% V_2O_5 (ZV) and ZnO with 0.5 mol% V_2O_5 and 0.5 mol% B_2O_3 (ZVB) ceramics are shown in Fig. 1. The XRD peaks originating from (100), (002), (101), (102), (110), (103), (200), (112), (201), (004) and (202) planes indicate that ZnO (JCPDS No. 36-1451) is a main phase for all samples. The samples exhibit sharp, well defined XRD peaks indicating good crystallinity and a reduction in the peaks intensities was observed only for the ZVB sample. In XRD pattern of the ZV sample, the small amount of $Zn_3(VO_4)_2$ (JCPDS No. 34-0378) phase was observed. The formation of $Zn_3(VO_4)_2$ phase in the V_2O_5-ZnO ceramic systems at 900 °C is coherent with previous studies in the literature [5,11,19,20]. There is also very small undefined peak in XRD pattern of the ZVB sample.

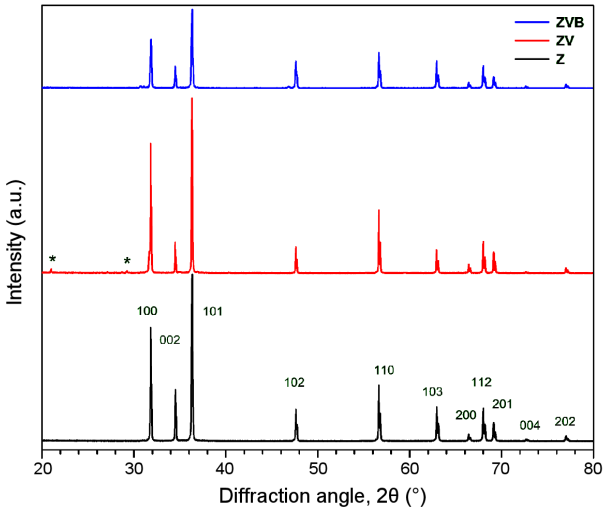

Figure 1. XRD patterns of Z, ZV and ZVB samples (* denotes $Zn_3(VO_4)_2$ phase)

Lattice parameter (a) was calculated to be 3.240, 3.2452 and 3.2429 Å for the Z, ZV and ZVB samples, respectively. It can be noticed that the pure zinc oxide sample (Z) has smaller a parameter value compared to its theoretical value (3.249 Å). This situation can be explained by the structural defects that may occur in the crystal structure of zinc oxide. According to theoretical calculations the lattice constants are a, b = 3.249 Å and c = 5.232 Å and average Zn–O bond length is 1.981 Å [21]. However, the room temperature lattice constants determined by different experimental measurements in the literature compared to theoretical calculations for ZnO are in good agreement. The lattice constants a and c were reported to be in the range of 3.24–3.25 Å and 5.20–5.21 Å, respectively [15,22]. Reason for a decrease in the lattice parameter is related to defect formation in ZnO. Oxygen vacancies might reduce the lattice parameters, at least the c value. On the other hand, formation of Zn_i interstitial defects lead to an increase in lattice constants [23,24]. These defects create donor states slightly below the conduction band. It is assumed that the donors are interstitial zinc ions Zn_i. The defect formation can be shown by Kröger-Vink notation:

$$Zn_i^x \longrightarrow Zn_i^{\cdot} + e' \quad (2)$$

$$Zn_i^{\cdot} \longrightarrow Zn_i^{\cdot\cdot} + e' \quad (3)$$

where $Zn_i^{\cdot}$ and $Zn_i^{\cdot\cdot}$ are single and double ionized interstitial zinc atoms, respectively [9]. In order to understand the formation of possible defects in the samples

in more detail, the samples were examined using the PL spectroscopy and will be discussed below.

It is reported that V_2O_5 can be partly dissolved into the ZnO matrix and V^{5+} ions enter the interstitial sites in ZnO [9]. The solubility of V_2O_5 was estimated to be ≤0.5 wt.% [25]. According to the substitutional reaction (Eq. 4), Zn^{2+} substitutions with vanadium ion (V_{Zn} is vanadium atom in zinc atom substitution site), released the free electrons and increased the conductivity [9]:

$$V_2O_5 \xrightarrow{ZnO} 2\,V_{Zn}^{\cdots} + 2\,O_O + \frac{3}{2}\,O_2 + 6\,e' \qquad (4)$$

Moreover, it was also reported that oxygen will be retained in V-doped ZnO lattice more than in the pure ZnO due to the higher valence state of vanadium. As a result, amount of oxygen vacancies, $V_O^{\cdot\cdot}$, should be reduced and amount of zinc replaced by V^{5+} or V^{4+} (creating $V_{Zn}^{\cdots}$ or $V_{Zn}^{\cdot\cdot}$ sites) should increase according to the Kröger-Vink notation:

$$2\,V^{5+/4+} + \frac{5}{4}\,O^{2-} + \frac{5}{4}\,V_O^{\cdot\cdot} \longrightarrow 2\,V^{\cdots/\cdot\cdot} + \frac{5}{4}\,O_O^x \qquad (5)$$

Thus, vanadium (V^{4+} or V^{5+}) incorporation can form defect states in between the conduction and valence bands of ZnO [26].

According to Srivastava *et al.* [26] the valence state of vanadium controls the oxygen content and lattice dimensions. It was reported that both V^{4+} and V^{5+} ions are more electropositive than Zn^{2+} ions. As a result number of oxygen vacancies can be reduced, and an expansion of lattice can be expected in $Zn_{1-x}V_xO$. On the other hand, the radii of both V^{4+} (0.60 Å) and V^{5+} (0.495 Å) are smaller than Zn^{2+} (0.74 Å). This results in the lattice distortion. The internal competition of increasing oxygen content and reducing effective crystal radius determines the direction of lattice expansion and contraction [27].

In our study, no peaks related to B_2O_3 were detected by XRD. This indicates that B_2O_3 formed a solid solution with ZnO. This can be attributed to the incorporation of B-ion in ZnO structure. It was reported that there may be three potential explanations related to how B can be incorporated into ZnO. One is that B occupies the octahedral interstice. This is because all octahedral voids are empty in the ZnO crystal structure. Furthermore, two other mechanisms are oxygen or zinc atoms exchange by boron, respectively. When the B atom substitutes in ZnO lattice, it creates lattice defects and results in an increase in the electron concentration with the defect reaction as follows:

$$B_2O_3 \xrightarrow{ZnO} 2\,B_{Zn}^{\cdot} + 2\,O_O + \frac{1}{2}\,O_2 + 2\,e' \qquad (6)$$

The radius of B^{3+} (0.27 Å) is smaller than that of O^{2-} (1.4 Å) and Zn^{2+} (0.74 Å). If the oxygen or zinc atoms were substituted by boron, the crystal plane spacing would reduce, leading to diffraction peaks shifting to higher angle [28]. Peng *et al.* [21] suggested that when replacing one zinc atom with one boron atom (as B_{Zn}), there should be change in the bond length since Zn–O is longer than B–O (1.526 Å) due to the smaller B^{3+} radius compared to Zn^{2+}. On one hand, the existence of zinc or oxygen vacancies in B-doped ZnO leads to a decrease in cell volume, on the other hand, the existence of interstitial Zn leads to a longer Zn–O length and an expansion in cell volume. The formation energy of Zn vacancy in un-doped ZnO is higher than that obtained for B-doped ZnO. This indicates that Zn vacancies form more easily in B-doped ZnO than in un-doped ZnO. These results are similar for oxygen vacancies, which mean that boron addition simplifies the formation of V_{Zn} and V_O [21]. Similar results have been reported in the literature, indicating that a higher number of oxygen vacancies or defects exist in B-doped ZnO than in un-doped ZnO [29].

FT-IR spectra of the Z, ZV and ZVB samples in the bandwidth of 400–1500 cm^{-1} representing the fingerprint region of samples are shown in Fig. 2. Metal oxides generally exhibit absorption bands in the fingerprint region (i.e. below 1000 cm^{-1}), which arise from interatomic vibrations [30]. According to Fig. 2, the peaks at 575 and 618 cm^{-1} indicate a stretching mode of Zn–O. Peaks at 758 and 1140 cm^{-1} can be attributed to the C–O bond stretching.

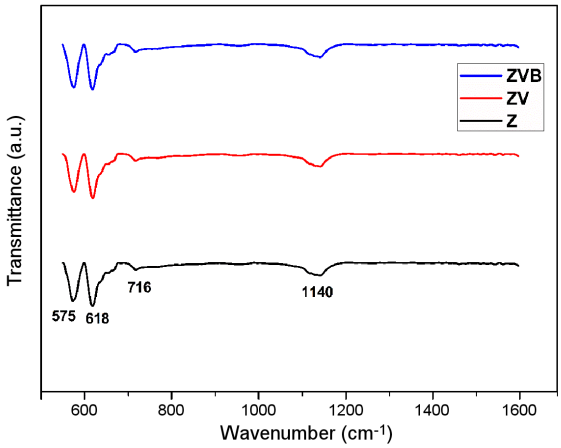

Figure 2. The FT-IR spectra for the Z, ZV and ZVB samples

Bulk densities of the Z, ZV and ZVB samples were 4.61, 5.47 and 5.42 g/cm^3, respectively. Figure 3 shows microstructure of the Z, ZV and ZVB samples. The average grain sizes are calculated by linear intercept method as described in our previous work [18]. Microstructure of the Z sample has very small grains with the average grain size of 3.5 μm. The addition of V_2O_5 to ZnO ceramics resulted in the increase of grain size and some of grains have oblong shape morphology. The average grain sizes of the ZV and ZVB samples calculated using linear intercept method are 9.0 and 18.4 μm, respectively. The addition of B_2O_3 to V_2O_5-ZnO ceramics results in further increase in grain size. The abnormal grain growth during sintering process is a com-

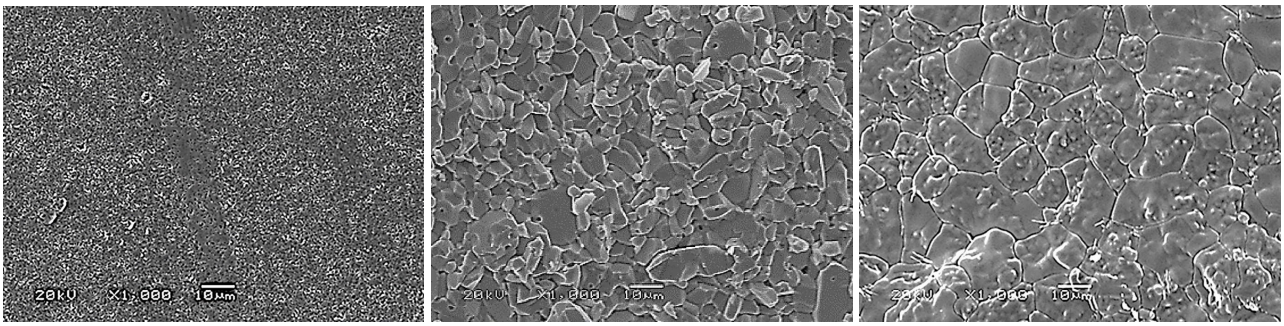

(a) (b) (c)

Figure 3. SEM micrographs of: a) Z, b) ZV and c) ZVB samples

mon phenomenon for the V_2O_5-ZnO ceramics system. Consistent with the previous study, an exaggerated ZnO grain growth was observed in the ZnO ceramics with V_2O_5 [31]. Highly reactive V-rich liquid phase is reason for abnormal grain growth during sintering. The formation of $Zn_3(VO_4)_2$ phase in ZnO-V_2O_5 ceramics acts as a liquid-phase sintering aid at high temperature. Small values of grain growth exponent and apparent activation energy are indicative of the faster coarsening speed of ceramic microstructures. For example, the grain growth exponent and apparent activation energy of ZnO-V_2O_5 binary system with less than 2 mol% V_2O_5 are only ~1.6 and ~90 kJ/mol, respectively, even smaller than 3 and ~224 kJ/mol for the un-doped ZnO ceramics [32].

Furthermore, an important change in the morphology with even a small amount of vanadium addition has been reported by Joshi *et al.* [33]. The distortion and increased activity of ZnO can be explained by the substitution of Zn^{2+} by V-ion thus resulting in the grain growth. Since the ionic radii mismatch is quite high, it causes significant increase in the particle size even at very small doping concentration [33].

The addition of B_2O_3 to V_2O_5-ZnO ceramics is the reason for further increase in grain size. The sample has uniform polygonal shaped grain morphology. The grain size of the ZVB sample is around 20–30 μm. The B_2O_3 addition has a beneficial effect on grain growth in ZnO. In our previous work, it was reported that the addition of B_2O_3 ≤1 mol% resulted in a decrease in the average kinetic grain growth exponent (n) values and an increase in the activation energy for the grain growth. When B_2O_3 addition was above 1 mol%, the formation of $Zn_3B_2O_6$ phase caused a rise in grain growth kinetic exponent and grain growth activation energy [18]. For this reason, the 0.5 mol% B_2O_3 addition was chosen as addition level in this study.

Low melting point of B_2O_3 (450 °C) is lower than that of the eutectic reaction between ZnO and $Zn_3(VO_4)_2$ around 890 °C. The addition of B_2O_3 improved the liquid-assisted sintering in the V_2O_5-ZnO ceramics. The low melting point of B_2O_3, together with the eutectic reaction, can promote grain growth by prolonged liquid phase sintering process. Similar observations were reported for the Y_2O_3 and B_2O_3-doped ZnO varistor ceramics [34].

The room temperature PL spectra of the Z, ZV and ZVB samples are shown in Fig. 4. As it can be seen, this spectrum revealed broad visible emission band because of impurities and defects in ZnO which are caused by oxygen vacancies, vanadium and boron addition, as well as zinc interstitials. This emission band between 450–750 nm includes the entire visible region from blue to red. Emissions from the PL spectra can be attributed to oxygen vacancies, oxygen antisite, interstitial oxygen, zinc vacancy, double ionized zinc vacancy and single ionized interstitial $Zn_i^{\cdot}$ [27,35–37].

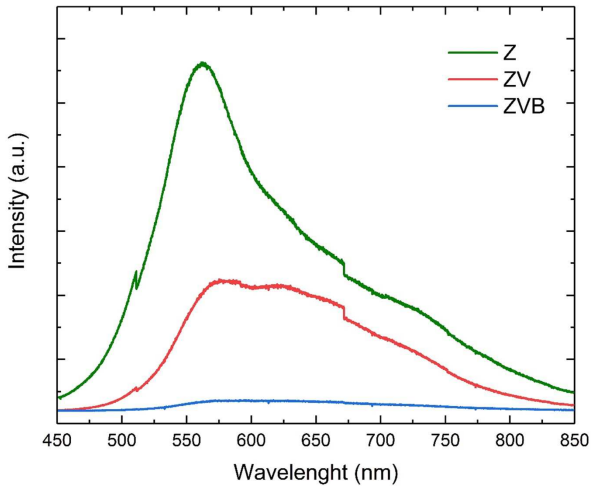

Figure 4. Room temperature PL spectra of Z, ZV and ZVB samples

To illustrate the physical process of the PL spectrum emission, we modelled all peaks using three emission lines, which are attributed to various defect states between the conduction band and the valence band of ZnO lattice (Fig. 5). In Fig. 5a, three emission peaks of the Z structure are shown. The peak emission energy for green, orange and red emissions were found at 562, 634 and 700 nm, respectively. As it can be seen (Fig. 5a), the highest emission was seen for green due to the oxygen vacancies and oxygen anti-site. In Fig. 5b three emission peaks of the ZV structure are shown. The peak emission energy for green, orange and red emissions were found at 567, 627 and 659 nm, respectively. As it can be seen, the green emission peak decreased, and the red emission peak increased compared to the pure Z. The red emis-

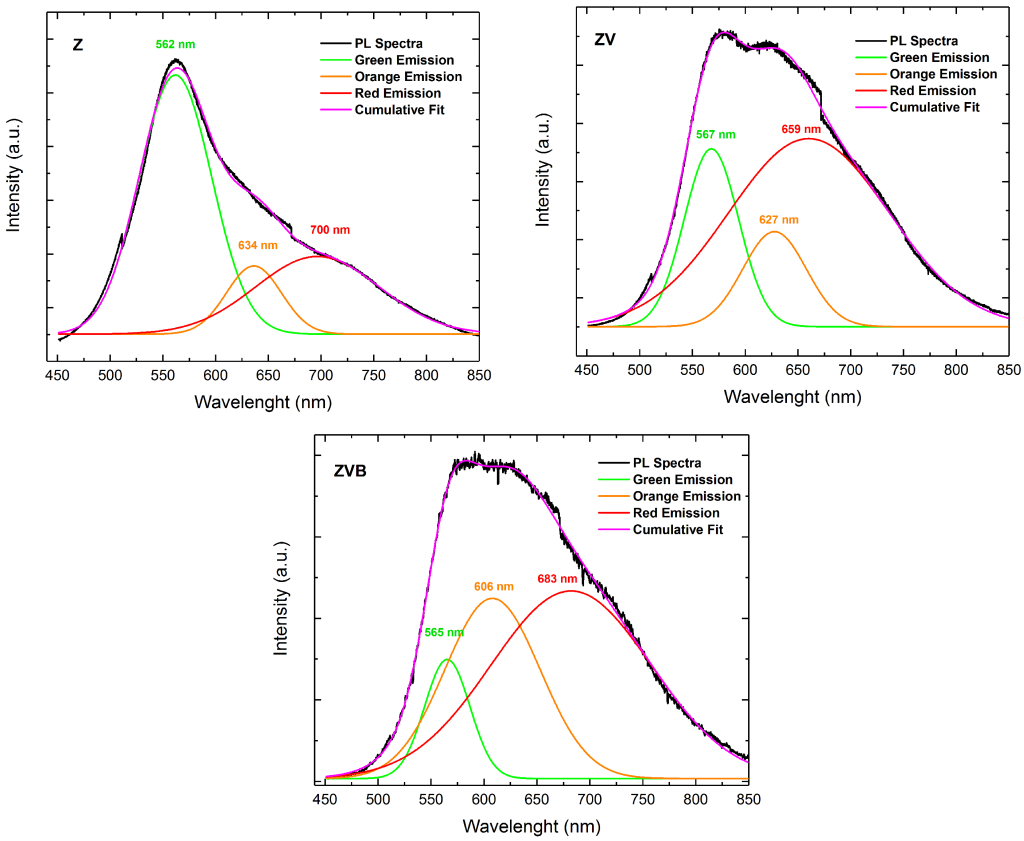

Figure 5. The peak emission energy of: a) Z, b) ZV and c) ZVB samples at room temperature

sion peak is about the same as the green emission due to interstitial zinc (Zn_i). In Fig. 5c three emission peaks of the ZVB structure are shown. The peak emission energy for green, orange and red emissions were found at 565, 606 and 683 nm, respectively. As it can be seen, the green emission peak decreased while the orange and red emission peaks increased compared to the other two structures due to Zn vacancies (V_{Zn}) and interstitial zinc (Zn_i). Reduced green emission, which is due to the oxygen vacancies, can be related to vanadium addition. As the higher charge dopant, vanadium substitution to zinc leads to the decrease in number of oxygen vacancies and thus suppression of green emission occurs in ZnO [27]. In line with XRD results further increase in zinc vacancy defect can be related to boron addition. As reported earlier, V_{Zn} form more easily in boron doped ZnO than in un-doped ZnO. Boron addition simplifies the formation of V_O and V_{Zn}. The presence of Zn or O vacancies in boron doped ZnO also leads to the shrinkage in lattice volume. In opposition, the presence of interstitial Zn leads to a longer Zn–O length and expansion in volume [19]. The internal competition of increasing defect species Zn_i, V_{Zn} and V_O decides the lattice expansion and contraction. This affects PL emission processes in the samples [27].

IV. Conclusions

The B_2O_3 and V_2O_5 dual addition to ZnO ceramics affects the structural properties remarkably. All samples exhibited main ZnO phase. Additionally, the small amount of $Zn_3(VO_4)_2$ phase was also observed in the ZnO containing 0.5 mol% V_2O_5 (ZV sample). The addition of V_2O_5 to ZnO ceramics gave rise to the increase in grain size and some of grains had oblong shape morphology. The abnormal grain growth during sintering process is a common phenomenon for the V_2O_5-ZnO ceramics system. The addition of B_2O_3 to V_2O_5-ZnO ceramics resulted in further increase in grain size. This sample had uniform polygonal shaped grain morphology. The room temperature PL spectra of the Z (ZnO), ZV (ZnO with 0.5 mol% V_2O_5) and ZVB (ZnO with 0.5 mol% V_2O_5 and 0.5 mol% B_2O_3) samples revealed broad visible emission band because of impurities and defects in ZnO which are caused by oxygen vacancies, vanadium and boron additions, as well as zinc interstitials. This emission band between 450–750 nm includes the entire visible region from blue to red. Our study revealed that the internal competition of increasing defect species Zn_i, V_{Zn} and V_O decides the lattice expansion and contraction which also affects PL emission processes in the samples. The ZVB ceramics can be sintered at a relatively low temperature (900 °C) which is attractive for many industrial applications. They can also be co-fired with a silver inner-electrode without using the expensive metals such as palladium or platinum.

Acknowledgement: This study was funded by Scientific Research Projects Coordination Unit of Istanbul University-Cerrahpaşa. Project number: 44313. This

study was supported by the Directorate of Presidential Strategy and Budget of Turkey (Project No. 2019K12-92587).

References

1. X. Fang, Y. Bando, U.K. Gautam, T. Zhai, H. Zeng, X. Xu, M. Liao, D. Golberg, "ZnO and ZnS nanostructures: ultraviolet-light emitters, lasers, and sensors", *Crit. Rev. Solid State Mater. Sci.*, **34** (2009) 190–223.
2. G. Biasotto, M.G.A. Ranieri, C.R. Foschini, A.Z. Simões, E. Longo, M.A. Zaghete, "Gas sensor applications of zinc oxide thin film grown by the polymeric precursor method", *Ceram. Int.*, **40** (2014) 14991–14996.
3. A. Apaolaza, D. Richard, M. R. Tejerina, "Experimental and ab initio study of the structural and optical properties of ZnO coatings: Performance of the DFT+U approach", *Process. Appl. Ceram.*, **14** [4] (2020) 362–371.
4. J.S. Dodds, F.N. Meyers, K.J. Loh, "Piezoelectric nanocomposite sensors assembled using zinc oxide nanoparticles and poly(vinylidene fluoride)", *Smart Struct. Syst.*, **12** (2013) 55-71.
5. H.H. Hng, P.L. Chan, "Cr_2O_3 doping in ZnO-0.5 mol% V_2O_5 varistor ceramics", *Ceram. Int.*, **35** (2009) 409–413.
6. H.H. Hng, K.Y. Tse, "Effects of MgO doping in ZnO-0.5 mol% V_2O_5 varistors", *Ceram. Int.*, **34** (2008) 1153–1157.
7. H.H. Hng, K.Y. Tse, "Grain growth of ZnO in binary ZnO-V_2O_5 ceramics", *J. Mater. Sci.*, **38** (2003) 2367–2372.
8. C.S. Chen, C.T. Kuo, T.B. Wu, I-N. Lin, "Microstructures and electrical properties of V_2O_5-based multicomponent ZnO varistors prepared by microwave sintering process", *Jpn. J. Appl. Phys.*, **36** (1997) 1169–1175.
9. M. Mirzayi, M.H. Hekmatshoar, "Effect of V_2O_5 on electrical and microstructural properties of ZnO ceramics", *Physica B*, **414**, (2013) 50–55.
10. H. Pfeiffer, K.M. Knowles, "Effects of vanadium and manganese concentrations on the composition, structure and electrical properties of ZnO-rich MnO_2-V_2O_5-ZnO varistors", *J. Eur. Ceram. Soc.*, **24** (2004) 1199–1203.
11. H.H. Hng, K.M. Knowles, "Characterisation of $Zn_3(VO_4)_2$ phases in V_2O_5-doped ZnO varistors", *J. Eur. Ceram. Soc.*, **19** (1999) 721–726.
12. R.A. Rakkesh, S. Balakumar, "Structural, electrical transport and optical studies of Li ion doped ZnO nanostructures", *Process. Appl. Ceram.*, **8** [1] (2014) 7–13.
13. J.C.A. Queiroz, J.B.A. Filho, J.Q.M. Neto, I.O. Nascimento, I.A. Souza, M.G.O. Queiroz, E.B. Melo, J.D.D. Melo, T.H.C. Costa, "Structural and optical properties of Al-doped ZnO thin films produced by magnetron sputtering", *Process. Appl. Ceram.*, **14** [2] (2020) 119–127.
14. S.W. Hwang, H.K. Kim, Y-H. Hwang, K-N. Koh, "A study of structures in ZnO and ZnO:V_2O_5 thin films by in-situ synchrotron X-ray scattering", *J. Korean Phys. Soc.*, **51** (2007) 862–865.
15. P. Shukla, J. K. Shukla, "Facile sol-gel synthesis and enhanced photocatalytic activity of the V_2O_5-ZnO nanoflakes", *J. Sci. Adv. Mater. Dev.*, **3** (2018) 452–455.
16. Q. Shi, S. Wang, H. Wu, M. Yu, X. Su, F. Ma, J. Jiang, "Synthesis and characterizations of V_2O_5/ZnO nanocomposites and enhanced photocatalytic activity", *Ferroelectrics*, **523** (2018) 74–81.
17. N.H. Nickel, E. Terukov, *Zinc Oxide - A Material for Micro- and Optoelectronic Applications*, Springer, Dordrecht, The Netherlands, 2005.
18. B. Yuksel, T.O. Ozkan, "Grain growth kinetics for B_2O_3-doped ZnO ceramics", *Mater. Sci. Poland*, **33** (2015) 220–229.
19. H-H. Hng, K.M. Knowles, "Microstructure and current-voltage characteristics of multicomponent vanadium-doped zinc oxide varistors", *J. Am. Ceram. Soc.*, **83** (2000) 2455–2462.
20. S. El-Rabaie, A.H. Khafagy, M.T. Dawoud, M.T. Attia "Mechanical, microstructure, and electrical properties of ternary ZnO-V_2O_5-Mn_3O_4 varistor with sintering temperature", *Bull. Mater. Sci.*, **38** (2015) 773–781.
21. Y-C. Peng, C-C. Chen, H-C. Wu, J-H. Lu, "First-principles calculations of electronic structure and optical properties of boron-doped ZnO with intrinsic defects", *Opt. Mater.*, **39** (2015) 34–39.
22. H. Morkoç, Ü. Özgür, *Zinc oxide fundamentals, materials and device technology*, Wiley-VCH Verlag GmbH & Co. KGaA, Weinheim, Germany, 2009.
23. X. Li, Y. Wang, W. Liu, G. Jiang, C. Zhu, "Study of oxygen vacancies influence on the lattice parameter in ZnO thin film", *Mater. Lett.*, **85** (2012) 25–28.
24. J.H. Park, Y.J. Lee, J-S. Bae, B-S. Kim, Y.C. Cho, C. Moriyoshi, Y. Kuroiwa, S. Lee, S-Y. Jeong, "Analysis of oxygen vacancy in Co-doped ZnO using the electron density distribution obtained using MEM", *Nanoscale Res. Lett.*, **10** (2015) 186.
25. F. Mendez-Martinez, M.J. Venegas, H. Pfeiffer, "Microstructural development of ZnO pellets doped with different vanadium oxides (V_2O_5 and V_2O_3)", *Int. J. Appl. Ceram. Technol.*, **4** (2007) 564–570.
26. T. Srivastava, G. Bajpai, G. Rathore, S. Biring, S. Sen, "Vanadium substitution: A simple and efficient way to improve UV sensing in ZnO", *J. Appl. Phys.*, **123** (2017) 161407.
27. T. Srivastava, G. Bajpai, N. Tiwari, D. Bhattacharya, S.N. Jha, S. Kumar, S. Biring, S. Sen, "Opto-electronic properties of $Zn_{(1-x)}V_xO$: green emission enhancement due to V^{4+} state", *J. Appl. Phys.*, **122** (2017) 025106.
28. W. Wang, T. Ai, Q. Yu, "Electrical and photocatalytic properties of boron-doped ZnO nanostructure grown on PET-ITO flexible substrates by hydrothermal method", *Sci. Rep.*, **7** (2017) 42615.
29. A.B. Patil, K.R. Patil, S.K. Pardeshi, "Enhancement of oxygen vacancies and solar photocatalytic activity of zinc oxide by incorporation of nonmetal", *J. Solid State Chem.*, **184** (2011) 3273–3279.
30. M.F. Khan A.H. Ansari, M. Hameedullah, E. Ahmad, F.M. Husain, Q. Zia, U. Baig, M.R. Zaheer, M.M. Alam, A.M. Khan, Z.A. Al Othman, I. Ahmad, G.M. Ashraf, G. Aliev, "Sol-gel synthesis of thorn-like ZnO nanoparticles endorsing mechanical stirring effect and their antimicrobial activities: Potential role as nano-antibiotics", *Sci. Rep.*, **6** (2016) 27689.
31. H.H. Hng, L. Halim, "Grain growth in sintered ZnO-1 mol% V_2O_5 ceramics", *Mater. Lett.*, **57** (2003) 1411–1416.
32. Z. Ming, S. Yu, T.C. Sheng, "Grain growth of ZnO-V_2O_5 based varistor ceramics with different antimony dopants", *J. Eur. Ceram. Soc.*, **31** (2011) 2331–2337.
33. R. Joshi, P. Kumar, A. Gaur, K. Asokan, "Structural, optical and ferroelectric properties of V doped ZnO", *Appl.*

Nanosci., **4** (2014) 53–536.
34. K. Cheng, H. Zhao, Y. Zhou, Q. Xie, "B_2O_3-and Y_2O_3-doped ZnO varistor ceramics: enhanced voltage gradient and nonlinear properties for UHV", *Mater. Sci. Semicond. Process.*, **123** (2021) 105590.
35. R. Abaira, T. Dammak, A. Matoussi, A. Younes, "Structural and optical properties of zinc oxide doped by V_2O_5 synthesized by solid-state reaction", *Superlattices Microstruct.*, **91** (2016) 365–374.
36. S. Dagher, A.I. Ayesh, N. Tit, Y. Haik, "Influence of reactant concentration on optical properties of ZnO nanoparticles", *Mater. Techn. Adv. Perform. Mater.*, **29** (2014) 7–82.
37. S.S. Zahirullah, J.J. Prince, P.F.H. Inbaraj, "Structural and optical properties of Cu-doped ZnO nanorods by silar method", *Mater. Techn. Adv. Perform. Mater.*, **32** [12] (2017) 755–763.